Journal of Biomolecular NMR, **26:** 131–137, 2003.
KLUWER/ESCOM

NMR structure of the ribosomal protein L23 from *Thermus thermophilus*

Anders Öhman[a,*,**], Alexey Rak[b], Maria Dontsova[b], Maria B. Garber[b] & Torleif Härd[a]
[a]*Department of Biotechnology, Royal Institute of Technology (KTH), SE–106 91 Stockholm, Sweden;* [b]*Institute of Protein Research, Russian Academy of Sciences, 142292 Pushchino, Moscow Region, Russia*

Received 26 November 2002; Accepted 14 February 2003

Key words: L23, NMR spectroscopy, protein structure, ribosome, translation

Abstract

The ribosomal protein L23 is a component of the large ribosomal subunit in which it is located close to the peptide exit tunnel. In this position L23 plays a central role both for protein secretion and folding. We have determined the solution structure of L23 from *Thermus thermophilus*. Uncomplexed L23 consists of a well-ordered part, with four anti-parallel β-strands and three α-helices connected as β-α-β-α-β-β-α, and a large and flexible loop inserted between the third and fourth β-strand. The observed topology is distantly related to previously known structures, primarily within the area of RNA biochemistry. A comparison with RNA-complexed crystal structures of L23 from *T. thermophilus*, *Deinococcus radiodurans* and *Haloarcula marismourtui*, shows that the conformation of the well-ordered part is very similar in the uncomplexed and complexed states. However, the flexible loop found in the uncomplexed solution structure forms a rigid extended structure in the complexed crystal structures as it interacts with rRNA and becomes part of the exit tunnel wall. Structural characteristics of importance for the interaction with rRNA and with the ribosomal protein L29, as well as the functional role of L23, are discussed.

Introduction

Protein synthesis takes place at the ribosome, a ribonucleoprotein complex divided into two subunits that in total contains one-third protein and two-thirds RNA. Structures at atomic resolution of the large subunit in *Deinococcus radiodurans* (Harms et al., 2002) and *Haloarcula marismortui* (Ban et al., 2000), as well as the whole ribosome of *Thermus thermophilus* (Yusupov et al., 2001), have revealed many fascinating structural features and significantly increased our understanding for the mechanisms of protein synthesis (Nissen et al., 2000). The large subunit contains the catalytic centre for peptide bond formation, the polypeptide exit tunnel, and is involved in the protein secretion and folding process, while the small subunit carries out the decoding and translocation process.

One component of the large subunit of the ribosome is the protein L23 (denoted L25 in some eucaryotes). The crystal structures of the ribosome complexes have shown that L23 is located close to the exit tunnel of the ribosome, and that it attains a mixed α/β-structure with an extended protein segment protruding into the exit tunnel. However, in archaeal and many eucaryotic species the extended segment is deleted and replaced with the small protein L39e. The known ribosome structures show that L23 interacts strongly with the third domain of 23S rRNA of the ribosome, as well as the ribosomal protein L29 (also denoted L35 in some eucaryotes), and that it also interacts weakly with the first domain of 23S rRNA (Ban et al., 2000). Although the function of L23 is not understood in detail, recent studies have demonstrated its involvement both in the protein secretion process (Pool et al., 2002) and in the folding process of the nascent polypeptide chain (Kramer et al., 2002). In both cases L23 works as a docking site or anchor for either the signal recognition particle or, in the latter case, the Trigger Factor chaperone.

*Present address: Department of Biochemistry, Umeå University, SE–901 87 Umeå, Sweden.
**To whom correspondence should be addressed. E-mail: anders.ohman@chem.umu.se

The present report describes the solution structure of the 96 amino acid protein L23 from *T. thermophilus*, as determined by NMR spectroscopy, and compares it with homologous proteins with regard to amino-acid sequence and tertiary structure. In addition, its RNA-binding properties and central role for the protein secretion and folding process is discussed.

Materials and methods

Cloning, expression and purification

The gene encoding L23 from *T. thermophilus* was cloned into the pET11c expression vector, and the protein was overproduced in *E. coli* strain BL21(DE3). Uniformly ^{15}N- or ^{15}N,^{13}C-labeled protein was produced by growing cells in M9 minimal medium containing $^{15}NH_4Cl$ (Martek) and ^{13}C-[D_6]glucose (Cambridge Isotopes) as desired, supplemented with 0.6–0.8 g l^{-1} (^{13}C),^{15}N-Isogrow (Isotec Inc.). Unlabeled protein was produced in Luria Bertani medium. Cultures were grown in chosen media, induced with 0.1 mM IPTG at an OD_{595} of ∼0.7, and grown for an additional 3 hours before harvesting. After cell resuspension, lysis (French Press) and centrifugation, L23 was found as a soluble protein in the supernatant. Pure protein was obtained after 10 min of heat treatment at 50 °C, where most of the *E. coli* protein precipitated, followed by ion exchange (CM-Sepharose, Amersham) and hydrophobic interaction (Butyl-Toyopead, Amersham) chromatography. The appropriate fractions were collected and the protein was precipitated with $(NH_4)_2SO_4$ and dialysed against the NMR-sample buffer, 50 mM KH_2PO_4, pH = 5.1, 200 mM $LiCl_2$. After concentration and addition of 10% (v/v) D_2O a typical NMR sample had a protein concentration of approximately 0.8 mM and a pH of 5.1.

NMR spectroscopy and spectral analysis

NMR experiments were carried out at 35° on either Bruker *AVANCE* spectrometers, operating at proton frequencies of 500 or 600 MHz, or on a Varian *INOVA*, operating at 800 MHz. All spectrometers were equipped with 5 mm triple-resonance pulsed-field z-gradient probes. The NMR-data were processed using NMRPipe (Delaglio et al., 1995) or XWIN-NMR (Bruker Biospin), both running on Silicon Graphics O_2 workstations. Assignment and integration of cross-peaks were made in Ansig for Windows (Helgstrand et al., 2000). The sequence specific resonance assignment of the ribosomal protein L23 followed the standard triple-resonance strategy for ^{13}C,^{15}N-labeled proteins. From the experiments CBCANH, CBCA(CO)NH, HNCO, and HSQC, recorded at 600 MHz, and HNCA and HN(CO)CA recorded at 500 MHz, backbone and partial side chain assignments were obtained. Side chain assignments were verified and extended using 2D clean-TOCSY and DQF-COSY and 3D ^{15}N-DIPSI-HSQC, C(CO)NH, HC(CO)NH, HCCH-COSY and HCCH-TOCSY experiments, all recorded at 600 MHz. Distance restraints were obtained from a 3D ^{15}N-edited NOESY experiment recorded at 600 MHz and a 3D ^{13}C-edited NOESY recorded at 800 MHz, both with a mixing time of 100 ms.

Dynamical properties of the peptide backbone were investigated using {^{1}H}-^{15}N steady state NOE experiments, recorded at 600 MHz in an interleaved manner. Steady-state NOE values were determined as ratios of peak-heights. In order to estimate the uncertainty, duplicate experiments were carried out.

Structural restraints

The analysis of the NOESY spectra resulted in a set of unambiguously assigned NOEs, calibrated to known distances found in both α-helical and β-sheet secondary structure elements and divided into three classes: Weak (1.8–5.5 Å), medium (1.8–3.6 Å) and strong (1.8–2.7 Å). By using an iterative combination of structure calculation and a set of unambiguous distance restraints, many ambiguous NOE cross-peaks were resolved and assigned. The obtained distance restraints were processed by AQUA to remove redundant restraints (Laskowski et al., 1996). Dihedral angle restraints were derived using the TALOS program (Cornilescu et al., 1999).

Structure calculation and analysis

Structures were calculated and analysed by using XPLOR (v. 3.851) running on SGI O_2 or Octane workstations, or on a Linux-controlled PC. Additional structural analysis, molecular graphics, calculation of surface accessibility and electrostatic surface potential were made using MOLMOL (Koradi et al., 1996).

A total number of 100 structures were calculated from the structural restraints, using the XPLOR-scripts sa.inp and refine.inp. The duration of the first high-temperature molecular dynamics step in the

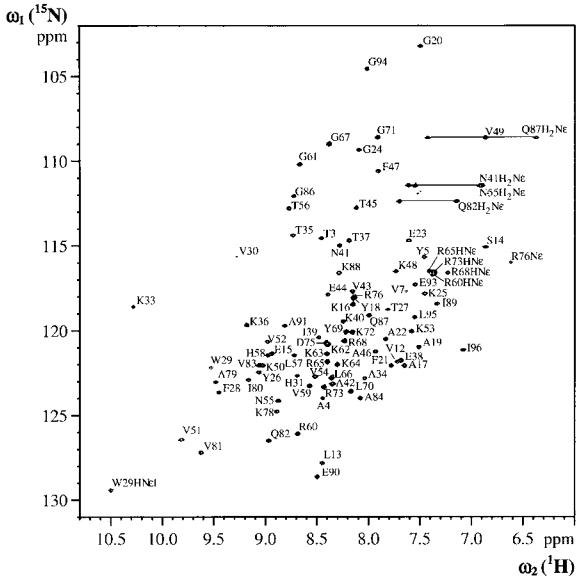

Figure 1. Assigned ^{1}H-^{15}N-HSQC spectrum of 0.8 mM sample of ^{15}N,^{13}C-labeled L23 from *T. thermophilus* recorded at 600 MHz (proton frequency) and 35 °C.

sa.inp protocol was increased to 45 ps, while the annealing step was increased to 20 ps. Similarily, the duration of the simulated annealing in the refinement protocol was increased to 45 ps. Distance restraints for non-stereo specifically assigned protons were included using r^{-6} summation (Fletcher et al., 1996).

The electrostatic potentials were calculated assuming point charges on heavy atoms, dielectric constants of 2 and 80 for protein and solvent, respectively, an ionic strength of 0.3 M, 2 Å salt radius and a boundary condition of zero potential at 10 Å. A solvent radius of 1.4 Å was used when the accessible van der Waals surfaces of the heavy atoms were identified, and when the relative solvent accessibility was determined.

Homology search

Sequence homologues and their alignment were found using the programs MaxHom (Sander and Schneider, 1991) and PSI-BLAST (Altschul et al., 1997), and visualised by using MView (Brown et al., 1998). A search for structurally homologous proteins among the structures deposited in the protein data bank was carried out using the programs DALI (Holm and Sanders, 1993) and TOP (Lu, 2000).

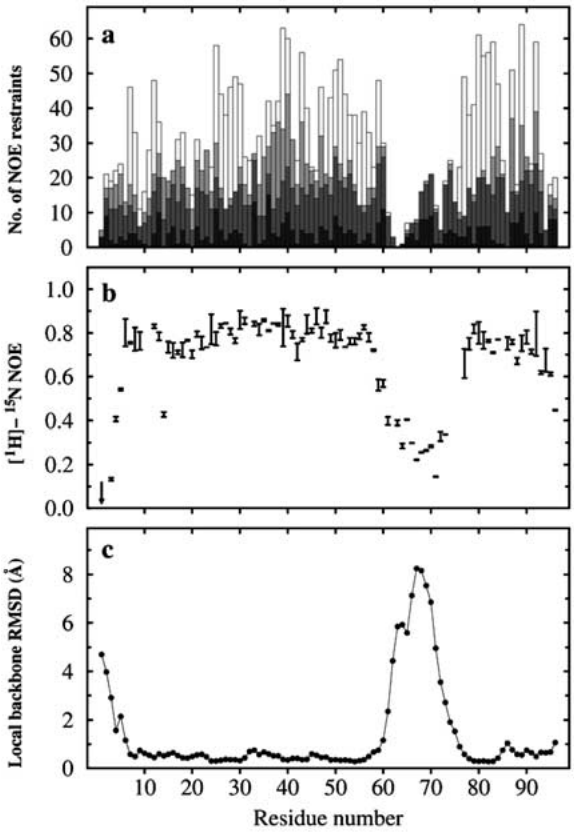

Figure 2. Structure precision and flexibility per residue of L23 from *T. thermophilus*: (a) Histogram of the number of non-redundant NOE-restraints used in the structure calculation. Intra-residual restraints are indicated with dark grey bars, sequential with medium grey, medium-range with light grey and long-range with open bars. (b) {^{1}H}-^{15}N steady state NOE measured at 600 MHz (proton frequency). Data points from two separate experiments are shown and connected with a riser. Residue 2 is not shown; it has an average NOE value of −0.52. (c) Average RMSD values per residue for the 29 structures in the final ensemble, versus the mean structure.

Results

NMR spectroscopy, spectral analysis and structure calculation

The quality of the data is illustrated in Figure 1, which shows the assigned ^{1}H,^{15}N-HSQC spectrum. Backbone assignments are essentially complete, the only exception being the amide nitrogen of Ala10. Furthermore, broadened and weak amide proton resonances, presumably due to conformational exchange, were observed for Asp6, Ile8, Leu9, Ala10, Lys77 and Leu92.

Nearly complete side chain resonance assignment is obtained. Assignments are missing only for a num-

Table 1. Structural statistics for the ensemble of 29 structures for L23 from *Thermus thermophilus*

Number of NOE-derived distance restraints		
Total number	1660	
Intraresidue	396	
Sequential ($\|i - j\| = 1$)	481	
Medium range ($2 \leq \|i - j\| \leq 4$)	280	
Long range ($\|i - j\| \geq 5$)	503	
Number of dihedral angle restraints		
Backbone ϕ-angle	61	
Backbone ψ-angle	41	
Average number of violations		
Distance restraints > 0.5 Å	0	± 0
> 0.2 Å	13.9	± 2.6
Dihedral angle restraints > 5°	0	± 0
Deviations from idealized covalent geometry		
Bonds (Å)	0.0030	± 0.0001
Angles (°)	0.59	± 0.02
Impropers (°)	0.46	± 0.02
Ramachandran plot analysis (residues 10–59,74–96)		
Residues in most favoured regions (%)	83.7	
Residues in additional allowed regions (%)	14.3	
Residues in generously allowed regions (%)	2.0	
Residues in disallowed regions (%)	0.0	
Atomic RMSD to the average structure (residues 10–59,74–96)		
Backbone heavy atoms (Å)	0.57	
All heavy atoms (Å)	0.97	

ber of arginines and lysines with overlapping resonances near random-coil chemical shifts, which is indicative of a localization close to the surface of or in a flexible part of the protein. Two residues, Tyr26 and Phe28, show upfield-shifted side-chain resonances.

A total number of 1660 non-redundant distance restraints were found, see Table 1, and the distribution of restraints along the peptide backbone is presented in Figure 2a. The average number of distance restraints per residue is 17, but it should be noted that the number of restraints, particularly long-range, involving residues 60–75, are few. A small number of ambiguous restraints, exclusively involving amide protons, were also included.

By using the program TALOS it was possible to obtain 41 pairs of backbone (ϕ,ψ) dihedral angle restraints (classified as Good by TALOS). An additional 20 ϕ-angles of nonglycine residues were restrained to negative values (Ludvigsen and Poulsen, 1992), based on weak intra-residual NOE connectivities between the H^N and H^α protons (Table 1).

Of the initial 100 structures, 55 were accepted using the criteria in the XPLOR script accept.inp (RMSD for bonds and angles less than 0.01 Å and 1°, respectively, no NOE violations larger than 0.5 Å and no dihedral angle restraint larger than 5°). The final ensemble of 29 structures was selected based on their energies and Ramachandran behaviour and have been deposited in the Protein Data Bank (PDB ID-code 1N88). Structural statistics are presented in Table 1.

Description of structure

The solution structure of L23 from *T. thermophilus* has both a well-ordered part, containing four anti-parallel β-strands and three α-helices, and a highly flexible part, consisting of a long loop, see Figures 3a and 3b. The connectivity scheme of the secondary structures is β-α-β-α-β-β-α. The N-terminal residues (Met1-Val7) are followed by the first β-strand (β1, Ile8-Pro11), a short loop (Val12-Ser14), the first α-helix (α1, Glu15-Phe21), a turn (Ala22-Gly24), the second β-strand (β2, Lys25-Val30) anti-parallel to β1, a loop (His31-Thr35), a long α-helix (α2, Lys36-Ala46), a turn (Phe47-Lys50), a third β-strand (β3, Val51-Val59) with a bulge at Val51 and Val52, a long disordered loop (Arg60-Asp75), the fourth β-strand (β4, Arg76-Val83) with a bulge at Val83 packed anti-parallel in between strand β2 and β3, a loop (Ala84-Ile89), one turn of α-helix (α3, Glu90-Glu93) and three fairly ordered C-terminal residues (Gly94-Ile96). As can be seen in Figures 3a and 3b, the structured part of L23 has a β-sheet that neatly wraps around the long second α-helix, while the first α-helix is located just at the edge on the other side of the β-sheet. The third α-helix packs between the other helices and the β-sheet. Notably, in six out of eight cases the β-strands end at either a glycine or a proline residue or at a neighbouring residue.

From the steady state NOE experiments (see Figure 2b) it is also clear that the long loop (Arg60-Asp75), the four N-terminal residues, Ser14 (located in a short loop) and the C-terminal residue, Ile96, show significant dynamics on short time scales. This agrees well with the RMSD values, although Ser14 and Ile96 show a rather limited flexibility, probably due to sterical hindrance of the well-defined structural parts in their vicinity.

Analysis of the solvent accessible surface of L23 shows that the hydrophobic core is built from residues in all of the secondary structure elements, see Figure 3e. The electrostatic surface potential of L23,

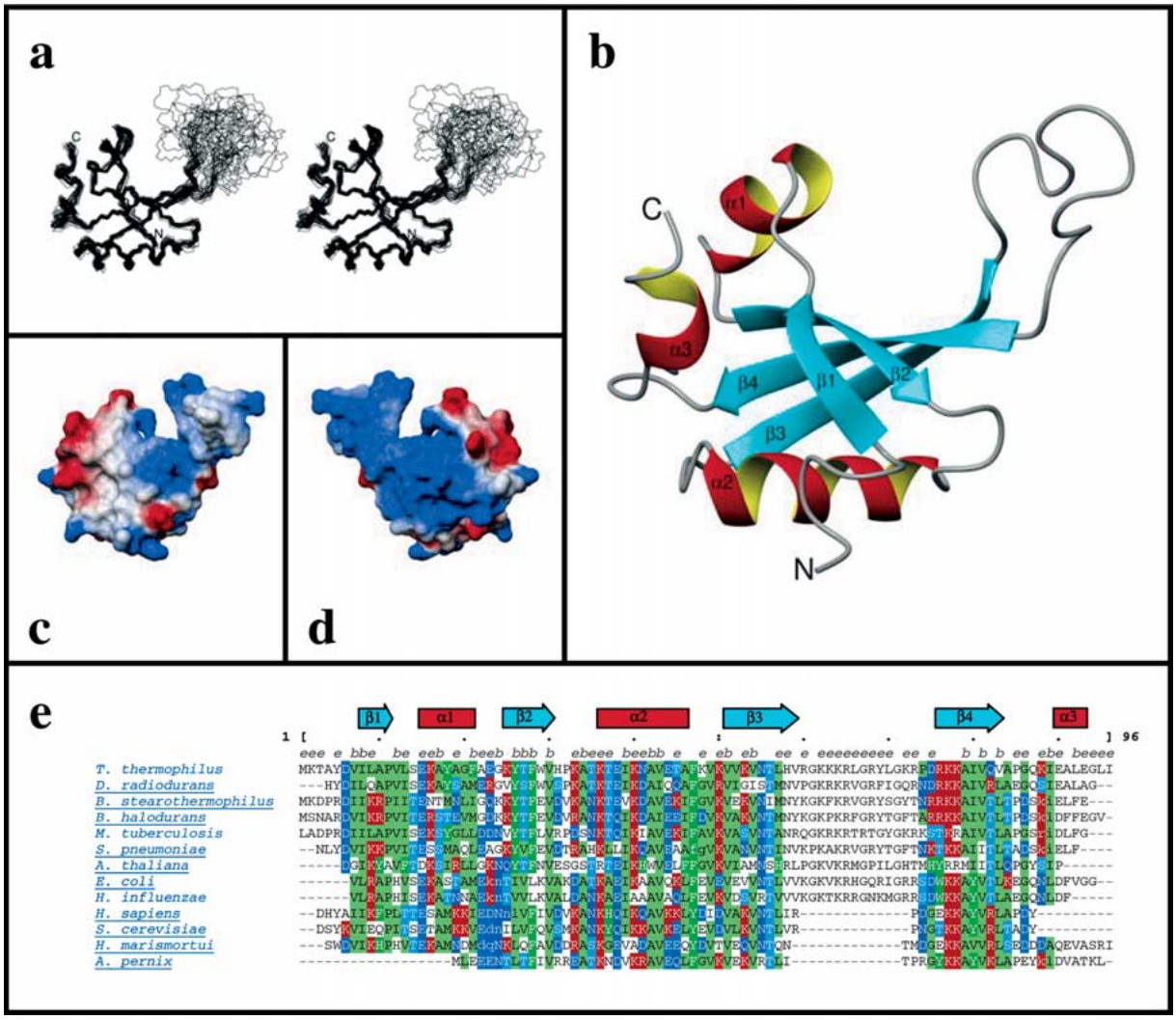

Figure 3. Solution structure and sequence comparison of the ribosomal protein L23 from *T. thermophilus*. (a) Stereo view showing the backbone atoms of residues 6–96 in the final ensemble of 29 calculated structures. Residues in the ordered regions (10–49, 74–96) are superimposed, and the N- and C-termini are indicated. (b) Ribbon representation of the lowest-energy structure in which the N- and C-termini as well as the secondary structure elements have been indicated. (c,d) Electrostatic surface potential of L23 from *T. thermophilus*, where blue and red represents positive and negative potential, respectively. The molecule in image (c) has the same orientation as in (b), whereas (d) is rotated 180° around a vertical axis. (e) Sequence alignment of a subset of selected L23 sequences, identified by their species name. Amino acids are colour-coded according to MView (Brown et al., 1998). The locations of β-sheet and α-helical secondary structure elements are indicated with arrows and boxes, respectively. Solvent accessible residues (>25% as determined with a 1.4 Å probe) are indicated by an *e*, buried (<5%) with a *b*. Images were prepared using MOLMOL (Koradi et al., 1996).

Figures 3c and 3d, shows that part of the disordered loop region and a nearby patch of the structured part, are highly positively charged. Notably, L23 also has a distinct negatively charged patch involving α-helix 1 and 3.

Sequence and tertiary homology

Sequence homologues to L23 from *T. thermophilus* were only found within the family of L23 proteins. The alignment of a selected number of sequences, representing a selection of bacterial, archaeal and eucaryotic species, is shown in Figure 3e. Many parts of the sequences were highly conserved, but for archaeal and many eucaryotic species a long stretch, corre-

sponding to residue 59 to 71 in L23 in *T. thermophilus*, is missing. A search for structurally homologous proteins, using Dali and TOP, resulted in a number of distantly homologous proteins. Most of these proteins are associated with RNA biochemistry. Two of the top-scoring proteins in both methods are RNA-binding domains from hnRNP A1 (Dali score 3.4; RMSD 3.2; PDB ID-code 1HA1) and the splicing factor U2Af (Dali score 3.1; RMSD 2.0; PDB ID-code 1U2F).

Discussion

The solution structure of L23 from *T. thermophilus* has a well-ordered part, consisting of four anti-parallel β-strands and three α-helices connected as β-α-β-α-β-β-α, as well as a highly flexible loop-region inserted between the third and fourth β-strand (Figure 3). The rigidity of the structured part and flexibility of the loop region is confirmed by the $\{^1H\}$-^{15}N steady state NOE results and RMSD values (Table 1, Figures 2b and 2c). A comparison between the well-ordered parts of the solution structure of L23 and corresponding parts of the complexed forms found in the crystal structures of *T. thermophilus*, *D. radiodurans* (60% sequence identity) and *H. marismortui* (29% sequence identity) shows a significant structural similarity with RMSD values for the CA-carbons of 0.78, 1.18 and 0.78 Å, respectively.

Inspection of the hydrophobic core of the structured part of the protein reveals that several residues have a high degree of conservation among species and probably are important for its stability (Figure 3e). Phe28 and Val30 are the most conserved residues, followed by Ile39, Ala42, Val51, Val54, Ala79 and to some extent Val81. The upfield-shifted resonances of the centrally located Tyr26 and Phe28 can be explained by ring-current shifts, due to aromatic residues in the vicinity, in particular Phe47. Another group of conserved hydrophobic residues, Gly24, Ala34, Val49 and Val83, are positioned at the edge of the hydrophobic core or in loops. However, in L23 from *T. thermophilus*, the consensus residue in position 24, Asn, is exchanged to a Gly, and in position 83 the consensus residue Leu is exchanged to a Val.

Even though the N-terminal part is poorly defined structurally, as judged from the $\{^1H\}$-^{15}N steady-state NOE experiments and RMSD values (Figures 2b and 2c), it does have several medium- and long-range NOEs (Figure 2a), and consequently only the first few amino acids can be considered to be disordered. Furthermore, several resonances in the N-terminal region are broadened, which indicates the occurrence of conformational exchange in this region. However, in complex with the ribosome the observed structural variability or conformational exchange of the N-terminal region is very likely absent due to the interaction, and a concomitant stabilization, with another ribosomal protein, L29. A more detailed inspection of the interaction between L23 and L29 in the structure of the large subunit of the ribosome from *D. radiodurans* shows that a number of residues appear to be important for their interaction. The corresponding residues in L23 from *T. thermophilus* are Tyr5, Ala10 and Pro11, of which Pro11 is well conserved in most species.

The flexible loop region found in the solution structure of L23 is, upon binding to the ribosome, likely to attain a well-defined extended conformation that is part of the exit tunnel (cf. Harms et al., 2001). Higher species, which lacks this region (Figure 3e), have replaced the extra stretch with a small protein denoted L39e, possibly because a tighter control of the exit tunnel is necessary. A search for sequence homologous to these extra residues, outside of the group of L23 proteins, showed a significant similarity to a stretch of residues in the families of calcium release channel proteins and elongation factor G (EF-G). The latter form a β-hairpin conformation (Ævarsson et al., 1994) and, interestingly, a very similar fold is observed for RNA-complexed L23 from *D. radiodurans*, a protein that has these extra residues (Harms et al., 2001).

Further investigation of the different ribosome structures shows that L23 interacts with RNA via the C-terminal part of β-strand 3 together with the long extended loop-region. In addition, positively charged residues in the N-terminal part of α-helix 1 and 2, as well as their preceding loops also interact with the nucleic acids. A number of charged or polar residues in these regions are well conserved among species, particularly the exposed and positively charged residues Lys36 and Lys40, but also the slightly less exposed positively charged Lys77 and polar Asn55. This cluster of residues and the loop region, create a positively charged patch well suited for the interaction with RNA, see Figures 3c and 3d. However, no known RNA-binding motif was identified.

A search for structurally related proteins were carried out by using Dali and TOP, and resulted in several distantly homologous proteins, usually involved in RNA biochemistry. The two top-scoring proteins, hnRNP A1 and U2Af, have a topology comparable with

the β-α-β-β-α topology found in L23 from *T. thermophilus*. These proteins also bind RNA but with a different RNA binding mode, primarily involving two β-sheets that would correspond to β2 and β4 in L23, and with consensus sequences not found in L23.

The function of L23 is not understood in detail, but its crucial position close to the exit tunnel of the ribosome initially suggested an involvement in the protein secretion process. One important study, which strengthened this suggestion, showed that a ribosomal protein complex of 21 kDa is involved in the process. This molecular weight corresponds well with a complex between L23 and L29, two proteins in contact close to the exit tunnel and known to interact from crosslinking studies (Fulga et al., 2001). A recent study finally identifies L23 as the anchor point for the signal recognition particle, positioning the particle in such a way that it can read the signal sequence of the nascent polypeptide (Pool et al., 2002). Another recent investigation has clearly shown that L23 can have one additional function as it provides a docking site for the Trigger Factor chaperone, thereby assisting in the protein folding process of newly synthesised polypeptides (Kramer et al., 2002). In the latter case, Glu15 (using the corresponding residue number in *T. thermophilus*), was clearly identified as the most important residue for the interaction. This highly conserved residue among the L23 proteins from various species is located at the beginning of α-helix 1 and well exposed with a crucial position close to the exit tunnel of the ribosome. Two more residues, Ser14 and Lys16, also show some conservation, and with their position next to Glu15 they may also play a functional role. An exposed negatively charged patch on the L23 protein (see Figure 3c), in the vicinity of both the exit channel of the ribosome and the conserved and functionally important Glu15, may also be of importance for its functional properties.

Accession numbers

The sequence specific resonance assignment has been deposited in the BioMagResBank (accession number BMRB-5650). Coordinates of the final ensemble of 29 structures have been deposited in the Protein Data Bank (PDB ID-code 1N88).

Acknowledgements

This work was supported by grants from the Swedish Natural Science Research Council (NFR), the Swedish

Royal Academy of Sciences (KVA), the Knut and Alice Wallenberg Foundation (KAW), the Russian Academy of Sciences and the Russian Foundation for Basic Research. M.G. was supported in part by an award from the Howard Hughes Medical Institute. The Swedish NMR Centre is acknowledged for allowing use of their 800 MHz NMR spectrometer.

References

Ævarsson A., Brazhnikov, E., Garber, M., Zheltonosova, J. Chirgadze, Y., Al-Haradaghi, S.A., Svensson, L.A. and Liljas, A. (1994) *EMBO J.*, **13**, 3669–3677.

Altschul, S.F., Madden, T.L., Schäffer, A.A., Zhang, J., Zhang, Z., Miller, W. and Lipman, D.J. (1997) *Nucl. Acids Res.*, **25**, 3389–3402.

Ban, N., Nissen, P., Hansen, J., Moore, P.B. and Steitz, T.A. (2000) *Science*, **289**, 905–920.

Brown, N.P., Leroy, C. and Sander C. (1998) *Bioinformatics*, **14**, 380–381.

Cornilescu, G., Delaglio, F. and Bax, A. (1999) *J. Biomol. NMR*, **13**, 289–302.

Delaglio, F., Grzesiek, S., Vuister, G., Zhu, G., Pfeifer, J. and Bax, A. (1995) *J. Biomol. NMR*, **6**, 277–293.

Fletcher, C.M., Jones, D.N.M., Diamond, R. and Neuhaus, D. (1996) *J. Mol. Biol.*, **8**, 292–310.

Fulga, T.A., Sinning, I., Dobberstein, B. and Pool, M.R. (2001) *EMBO J.*, **20**, 2338–2347.

Harms, J., Schluenzen, F., Zarivach, R., Bashan, A., Gat, S., Agmon, I., Bartels, H., Franceschi, F. and Yonath, A. (2001) *Cell*, **107**, 679–688.

Helgstrand, M., Kraulis, P., Allard, P. and Härd, T. (2000) *J. Biomol. NMR*, **18**, 329–336.

Holm, L. and Sander, C. (1993) *J. Mol. Biol.*, **233**, 123–138.

Koradi, R., Billeter, M. and Wüthrich, K. (1996) *J. Mol. Graphics*, **14**, 51–55.

Kramer, G., Rauch, T., Rist, W., Vorderwülbecke, S., Patzelt, H., Schulze-Specking, A., Ban, N., Deuerling, E. and Bukau, B. (2002) *Nature*, **419**, 171–174.

Laskowski, R.A., Rullmann, J.A.C., MacArthur, M.W., Kaptein, R. and Thornton, J.M. (1996) *J. Biomol. NMR*, **8**, 477–486.

Lu, G. (2000) *J. Appl. Cryst.*, **33**, 176–183.

Ludvigsen, S. and Poulsen, F.M. (1992) *J. Biomol. NMR.* **2**, 227–233.

Nissen, P., Hansen, J., Ban, N., Moore, P.B. and Steitz, T.A. (2000) *Science*, **289**, 920–930.

Pool, M.R., Stumm, J., Fulga, T.A. Sinning, I. and Dobberstein, B. (2002) *Science*, **297**, 1345–1348.

Sander, C. and Schneider, R. (1991) *Proteins*, **9**, 56–68.

Yusupov, M.M., Yusupova, G.Z., Baucom, A., Lieberman, K., Earnest, T.N., Cate, J.H.D. and Noller, H.F. (2001) *Science*, **292**, 883–896.